

# An Adaptive Periodic-Disturbance Observer for Periodic-Disturbance Suppression

Hisayoshi Muramatsu, *Student Member, IEEE*, and Seiichiro Katsura, *Member, IEEE*

**Abstract**—Repetitive operations are widely conducted by automatic machines in industry. Periodic disturbances induced by the repetitive operations must be compensated to achieve precise functioning. In this paper, a periodic-disturbance observer (PDOB) based on the disturbance observer (DOB) structure is proposed. The PDOB compensates a periodic disturbance including the fundamental wave and harmonics by using a time delay element. Furthermore, an adaptive PDOB is proposed for the compensation of frequency-varying periodic disturbances. An adaptive notch filter (ANF) is used in the adaptive PDOB to estimate the fundamental frequency of the periodic disturbance. Simulations compare the proposed methods with a repetitive controller (RC) and the DOB. Practical performances are validated in experiments using a multi-axis manipulator. The proposal provides a new framework based on the DOB structure to design controllers using a time delay element.

**Index Terms**—Periodic disturbance, disturbance observer, adaptive notch filter, time delay element, adaptive control

## I. INTRODUCTION

PERIODIC motions are usual industrial tasks in operations using automatic systems. For example, actuators, automatic machines, and robots are used because of their high precision, high speed, and their capability to work for long hours. However, most repetitive activities induce periodic disturbances that consist of a fundamental wave and harmonics. In order to realize precise periodic motions, periodic-disturbance suppression considering the fundamental wave and harmonics is a problem to be solved.

A disturbance observer (DOB) is a two-degree-of-freedom controller based on an observer structure for suppressing disturbances [1]–[4]. The two-degree-of-freedom structure can only control the disturbance suppression to not affect the tracking ability. The DOB has a Q-filter  $Q(z^{-1})$  that determines the sensitivity function  $Q(z^{-1})z^{-1}$  and the complementary sensitivity function  $1 - Q(z^{-1})z^{-1}$  of the DOB. The Q-filter is typically set to a low-pass filter to realize high-pass sensitivity and low-pass complementary sensitivity on the basis of a tradeoff between the functions because the sensitivity characteristic enables disturbance suppression and the complementary sensitivity characteristic corresponds

to noise sensitivity and robust stability [5], [6]. However, the high-pass characteristic is not suitable to compensate a periodic disturbance because it possesses powers only at an infinite number of specific frequencies. To suppress the periodic disturbance, DOB-based controllers and high-order DOBs have been studied by focusing on some specific high-frequency waves [7], [8]. In [9], a periodic adaptive disturbance observer was proposed that consists of searching and learning phases and considers harmonics. A typical DOB is only used in the searching phase as an initial condition for the learning phase. Hence, it does not use the advantages of a DOB structure in the learning phase to compensate disturbances. Since the method (which also affects the tracking characteristic) is not the two-degree-of-freedom controller, it is more similar to a repetitive controller (RC) rather than to a DOB.

Repetitive control is a well-known method that focuses on suppressing all frequencies of a periodic disturbance [10]–[12]. The RC improves both tracking performance regarding a periodic signal and suppression performance on an exogenous periodic signal by using a time delay element. However, RCs have the following three problems. First, the time delay element interferes with the command-tracking characteristic and the nominal stability. Second, the sensitivity characteristic amplifies other disturbances such as aperiodic disturbances. Finally, the complementary sensitivity function is not sufficiently designed.

RCs using a DOB structure have been studied [13]. In [14], attenuating the amplification of other disturbances was achieved. However, the bandwidth of the band-stop characteristics suppressing periodic disturbances is narrow, and the command-tracking characteristic and the nominal stability are still affected by the time delay element.

In this paper, a periodic disturbance observer (PDOB) is proposed. It contributes a simultaneous realization of the characteristics, which solves the above-mentioned problems.

- 1) The PDOB including a time delay element aims at compensating all frequencies of a periodic disturbance with an infinite number of band-stop characteristics.
- 2) The time delay element does not affect the nominal stability.
- 3) The PDOB does not affect the nominal command-tracking characteristic.
- 4) The amplification of other disturbances can be attenuated by the sensitivity function adjusted by a design parameter  $\gamma$ .
- 5) The parameter  $\gamma$  can also adjust the complementary sensitivity function.

©2018 IEEE.

Manuscript received September 26, 2017; revised December 12, 2017; accepted December 27, 2017. Date of publication February 9, 2018; date of current version October 3, 2018.

H. Muramatsu and S. Katsura are with the Department of System Design Engineering, Keio University, Yokohama 223-8522, Japan (e-mail: muramatsu@katsura.sd.keio.ac.jp; katsura@sd.keio.ac.jp).

The published version of the paper is available online at <https://ieeexplore.ieee.org/abstract/document/8288655>

Digital Object Identifier 10.1109/TII.2018.2804338

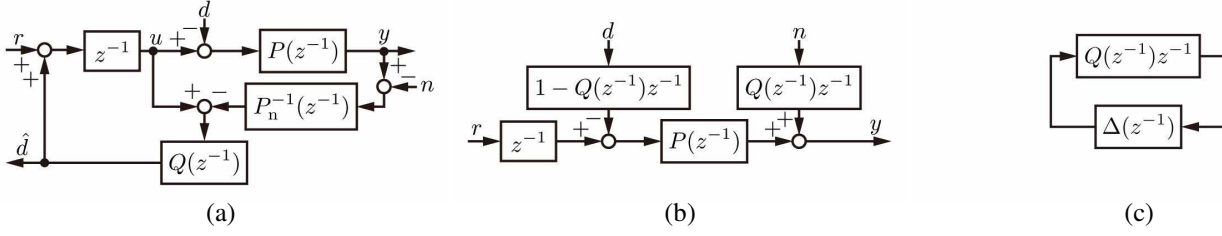


Fig. 1. (a) Block diagram of general DOB. (b) Equivalent Block diagram of DOB for  $\Delta(z^{-1}) = 0$ . (c) Equivalent Block diagram of DOB for small-gain theorem.

6) Implementation is simple because of using the time delay element.

The PDOB achieves performance by focusing only on periodic-disturbance suppression. Thus, it can estimate and compensate periodic disturbances more effectively than conventional DOBs because the PDOB uses a time delay element considering the dynamics of a periodic disturbance. Further, owing to the integration of the time delay element, the PDOB leads better results regarding periodic disturbances than other conventional disturbance estimation methods, e.g., active disturbance rejection control and an uncertainty-and-disturbance estimator [15], [16].

Moreover, deterioration of the suppression performance due to, e.g., identification errors, unknown frequencies, or varying frequencies is also an important problem [17], [18]. To solve problems due to uncertainties, adaptive control is a typical approach [19], [20]. This paper specifically addresses adaptive estimation of a fundamental frequency regarding a periodic disturbance. In recent years, adaptive rejection of several sinusoidal disturbances [21] and RCs based on a multiple-memory-loop technique broadening the bandwidth [22] have been studied. This paper proposes an adaptive PDOB in addition to the PDOB to compensate also frequency-varying periodic disturbances. Since adaptive notch filters (ANFs) are well-known frequency estimators regarding periodic signals [23], [24], the adaptive PDOB employs an ANF that is designed to estimate a fundamental frequency from a periodic disturbance including harmonics. The adaptive PDOB acquires adaptivity through the design of six additional design parameters.

## II. PERIODIC-DISTURBANCE OBSERVER

### A. Q-filter and Transfer Functions

A disturbance  $d(k)$  is defined as a composition of a periodic disturbance  $d_p(k)$  and an aperiodic disturbance  $d_a(k)$

$$d(k) = d_p(k) + d_a(k).$$

The dynamics of the periodic disturbance are defined by

$$d_p(k) = d_p(k - N) + \rho(k),$$

where

$$\rho(k) = \begin{cases} \rho_0(k) & k < N \\ 0 & N \leq k \end{cases}. \quad (1)$$

$\rho_0(k)$  and  $N$  are the initial wave and delay, respectively. The Z-transformed periodic disturbance is

$$d_p(z^{-1}) = \frac{1}{1 - z^{-N}} \rho(z^{-1}).$$

Fig. 1 shows a block diagram and its equivalents of a general DOB.  $r$ ,  $n$ ,  $y$ ,  $u$ ,  $\hat{d}$ ,  $P$ ,  $P_n$ , and  $\Delta$  denote the reference, noise, output, input, estimated value, plant, nominal plant, and modeling error, respectively. Regarding Fig. 1(b), the periodic disturbance is compensated by the DOB with  $\frac{1 - Q(z^{-1})z^{-1}}{1 - z^{-N}} \rho(z^{-1})$ . Since  $\rho(k)$  is zero for  $N \leq k$ , the Q-filter satisfying

$$\frac{1 - Q(z^{-1})z^{-1}}{1 - z^{-N}} \rho(z^{-1}) = \gamma \rho(z^{-1})$$

suppresses the periodic disturbance for  $N \leq k$ . The design parameter  $\gamma$  is an integer. The Q-filter of the PDOB is calculated as

$$Q(z^{-1}) = q(z^{-1}) \{1 - \gamma(1 - z^{-N})\}, \quad (2)$$

where a low-pass filter  $q(z^{-1})$  is added to improve robust stability and the Z-operator  $z^{-1}$  is ignored to be a causal filter. In this paper, the low-pass filter  $q(z^{-1})$  is set to a first-order low-pass filter with

$$q(e^{-j\omega T_s}) = \frac{g}{g + j\omega}, \quad (3)$$

where  $g$  denotes the cutoff frequency. The PDOB implementation requires the inverse-nominal-plant model  $P_n^{-1}$  and the three parameters: delay  $N$ , design parameter  $\gamma$ , and cutoff frequency  $g$ .

The effects of the low-pass filter  $q(z^{-1})$  on the sensitivity and complementary sensitivity functions are shown in Fig. 2. The periodic-disturbance suppression and the robust stability are a tradeoff of both functions. The low-pass filter is added to improve the complementary sensitivity function in the high-frequency range, as shown in Fig. 2(b). The band-stop characteristics attenuated by the tradeoff are sufficient to compensate a periodic disturbance, as shown in Fig. 2(a). It is because most real harmonics become weak in the high-frequency range. The application of a high-order low-pass filter could improve the performance of the PDOB. However, this study employs a first-order low-pass filter to demonstrate fundamental characteristics of the proposed methods.

The nine transfer functions regarding Fig. 1(a) with  $r$ ,  $d$ , and  $n$  to  $y$ ,  $u$ , and  $\hat{d}$  are displayed in (4). In the functions, the nominal plant  $P_n(z^{-1})$  and the Q-filter  $Q(z^{-1})$  are expressed by the ratios of the coprime polynomials  $\frac{N_P(z^{-1})}{D_P(z^{-1})}$  and  $\frac{N_Q(z^{-1})}{D_Q(z^{-1})}$ , respectively. The modeling error  $\Delta(z^{-1})$  is defined by

$$P(z^{-1}) = \{1 + \Delta(z^{-1})\} P_n(z^{-1}).$$

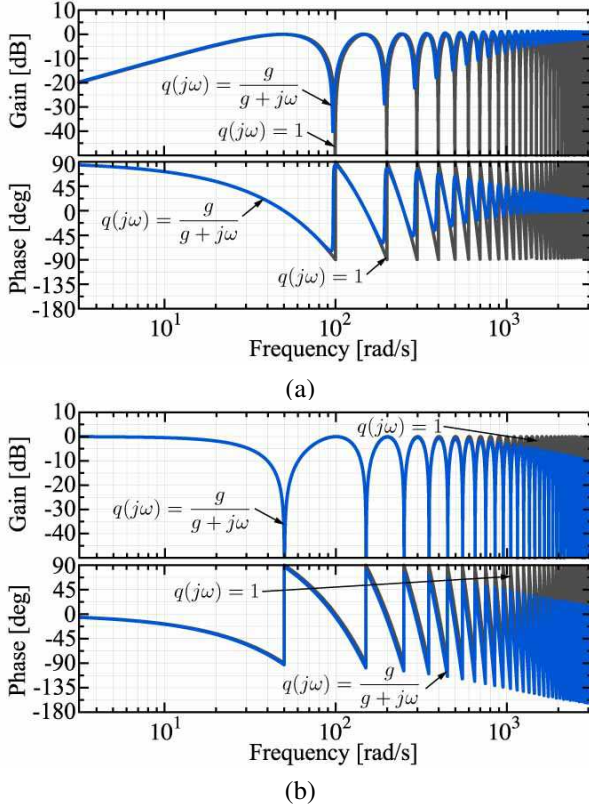


Fig. 2. Effect of low-pass filter  $q(z^{-1})$  on sensitivity and complementary sensitivity functions. The parameters are  $N = 2\pi/(\omega_0 T_k)$ ,  $\omega_0 = 100$  rad/s,  $\gamma = 0.5$ ,  $g = 1000$  rad/s, and  $T_k = 0.01$  ms. (a) Sensitivity functions of PDOB,  $1 - Q(z^{-1})z^{-1}$ . (b) Complementary sensitivity functions of PDOB,  $Q(z^{-1})z^{-1}$ .

The characteristic equation is

$$\phi(z^{-1}) = N_P D_P (D_Q + N_Q \Delta z^{-1}). \quad (5)$$

### B. Parameter Design

1) *Nominal Stability*: Under a nominal condition,  $\Delta(z^{-1}) = 0$ , the characteristic equation in (5) becomes

$$\phi_n(z^{-1}) = N_P D_P D_Q.$$

Since the polynomials of the Q-filter are  $N_Q(z^{-1}) = N_q(z^{-1})\{1 - \gamma(1 - z^{-N})\}$  and  $D_Q(z^{-1}) = D_q(z^{-1})$  with the ratio of the coprime polynomials of the low-pass filter,  $q(z^{-1}) = \frac{N_q(z^{-1})}{D_q(z^{-1})}$ , the nominal stability of the PDOB depends only on the stabilities of the three elements: zeros of nominal plant  $N_P$ , poles of nominal plant  $D_P$ , and poles of the low-pass filter  $D_Q$ . As a major characteristic of the PDOB, the nominal stability is independent of the delay  $z^{-N}$ .

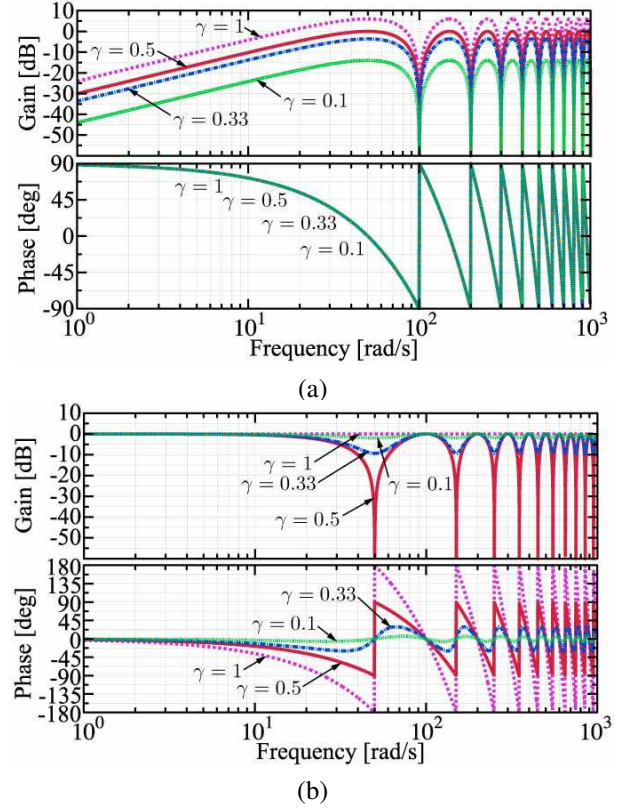


Fig. 3. Sensitivity and complementary sensitivity functions with variations in  $\gamma$ . The parameters are  $N = 2\pi/(\omega_0 T_k)$ ,  $\omega_0 = 100$  rad/s,  $q(z^{-1}) = 1$ , and  $T_k = 0.01$  ms. (a) Sensitivity functions of PDOB,  $1 - Q(z^{-1})z^{-1}$ . (b) Complementary sensitivity functions of PDOB,  $Q(z^{-1})z^{-1}$ .

2) *Calculation of  $N$* : The delay can be calculated with  $N = \frac{2\pi}{T_k \omega_0}$  considering the relation between period and angular frequency.  $T_k$  and  $\omega_0$  denote the sampling time and fundamental frequency, respectively. However, the added low-pass filter  $q(z^{-1})$  shifts the band-stop frequencies of  $1 - Q(z^{-1})z^{-1}$ , as shown in Fig. 2(a), instead of improving  $Q(z^{-1})z^{-1}$  (Fig. 2(b)). To correct the frequencies,  $N$  is modified with

$$N = \frac{2\pi g \gamma - \omega_0}{T_k g \omega_0 \gamma}. \quad (6)$$

The derivation is as follows. First, a correct delay  $N$  is defined as

$$N = \frac{2\pi}{T_k \omega_0} (1 + \sigma), \quad (7)$$

where  $\sigma$  is a small variation. Obtaining a fundamental frequency that causes the sensitivity function of zero,  $1 - e^{-j\omega_0 T_k} Q(e^{-j\omega_0 T_k}) = 0$ , is the objective, and it is rewritten by substituting the Q-filter in (2) as

$$\frac{g\gamma(1 - e^{-j\omega_0 T_k N}) + j\omega_0}{g + j\omega_0} = 0,$$

$$\begin{bmatrix} y \\ u \\ \hat{d} \end{bmatrix} = \frac{1}{\phi} \begin{bmatrix} N_P^2 D_Q (1 + \Delta) z^{-1} & -N_P^2 (D_Q - N_Q z^{-1}) (1 + \Delta) & N_P N_Q D_P (1 + \Delta) z^{-1} \\ N_P D_P D_Q z^{-1} & N_P N_Q D_P (1 + \Delta) z^{-1} & N_Q D_P^2 z^{-1} \\ -N_P N_Q \Delta D_P z^{-1} & N_P N_Q D_P (1 + \Delta) & N_Q D_P^2 \end{bmatrix} \begin{bmatrix} r \\ d \\ n \end{bmatrix} \quad (4)$$

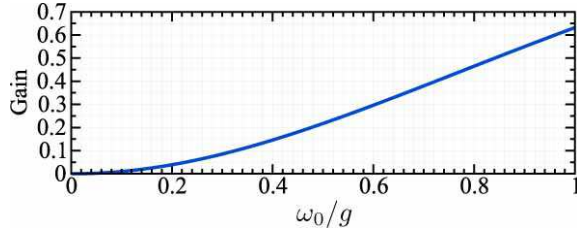


Fig. 4. Gain variation of (9) with respect to  $\omega_0/g$  at the fundamental frequency.

where  $z^{-1}$  is neglected. The rewritten objective becomes

$$2\pi g\gamma\sigma + \omega_0 = 0 \quad (8)$$

with the approximation of the time delay element

$$e^{-j\omega_0 T_k N} = e^{-j2\pi} e^{-j2\pi\sigma} = e^{-j2\pi\sigma} \approx 1 - j2\pi\sigma$$

based on (7) and the small variation  $\sigma$  satisfying  $|2\pi\sigma| < 1$ . The larger  $g$  is compared to  $\omega_0$ , the smaller is  $\sigma$ . The modified delay calculation in (6) is obtained by (7) and (8).

3) *Design of  $\gamma$* : The low-pass filter is set to  $q(z^{-1}) = 1$  and the Z-operators  $z^{-1}$  in  $1 - Q(z^{-1})z^{-1}$  and  $Q(z^{-1})z^{-1}$  are neglected to simplify the design of  $\gamma$ . The design parameter  $\gamma$  especially affects  $1 - Q(z^{-1})$  and  $Q(z^{-1})$  at the frequencies  $\omega_{b1}$  and  $\omega_{b2}$  with

$$\omega_{b1} = (2n)\frac{\omega_0}{2}, \quad \omega_{b2} = (2n+1)\frac{\omega_0}{2}, \quad n = 0, 1, 2, \dots,$$

as shown in Fig. 3. The gains of the functions

$$|1 - Q(e^{-j\omega T_k})| = \left| 2\gamma \sin\left(-\frac{NT_k\omega}{2}\right) \right|,$$

$$|Q(e^{-j\omega T_k})| = \left| \sqrt{1 + 4\gamma(\gamma - 1)\sin^2\left(-\frac{NT_k\omega}{2}\right)} \right|$$

become as follows for the frequencies  $\omega_{b1}$  and  $\omega_{b2}$

$$|1 - Q(e^{-j\omega_{b1} T_k})| = 0, \quad |1 - Q(e^{-j\omega_{b2} T_k})| = |2\gamma|,$$

$$|Q(e^{-j\omega_{b1} T_k})| = 1, \quad |Q(e^{-j\omega_{b2} T_k})| = |1 - 2\gamma|.$$

Considering an optimal complementary sensitivity characteristic,  $\gamma$  can be set to 0.5 to minimize  $|Q(e^{-j\omega_{b2} T_k})| = |1 - 2\gamma|$ .

4) *Design of  $g$* : The design parameter  $\gamma$  is set to 0.5 and the Z-operators  $z^{-1}$  in  $1 - Q(z^{-1})z^{-1}$  and  $Q(z^{-1})z^{-1}$  are neglected to simplify the design of  $g$ . The cutoff frequency  $g$  of (3) is designed in accordance with two objectives: periodic-disturbance suppression and robust stability. First, a lower limit for  $g$  is given by the fundamental-wave suppression performance. At the fundamental frequency, the gain of  $1 - Q(e^{-j\omega_0 T_k})$  using (6) is

$$|1 - Q(e^{-j\omega_0 T_k})| = \sqrt{\frac{\{1 - \cos(2\mu)\} + 2\mu\{\mu - \sin(2\mu)\}}{2(1 + \mu^2)}}, \quad (9)$$

where  $\mu = \omega_0/g$ . The gain depends only on  $\omega_0/g$ . Fig. 4 shows the gain variation with respect to  $\omega_0/g$ . An upper limit for  $\omega_0/g$  can be determined with the required precision and Fig. 4. Since the fundamental frequency  $\omega_0$  is given by a target

periodic-disturbance, the lower limit for  $g$  is obtained from the upper limit for  $\omega_0/g$ .

Next, an upper limit for  $g$  is derived in accordance with the robust stability using the equivalent block diagram of the PDOB for the small-gain theorem shown in Fig. 1(c). The modeling error consists of the weighting function  $W(z^{-1})$  and the variation  $\delta(z^{-1})$

$$\Delta(z^{-1}) = W(z^{-1})\delta(z^{-1}),$$

where the variation satisfies

$$\|\delta(z^{-1})\|_\infty \leq 1.$$

By assuming that the nominal PDOB and modeling error are stable, the robust-stability condition based on the small-gain theorem is

$$\|W(z^{-1})Q(z^{-1})z^{-1}\|_\infty < 1.$$

It can be rewritten as

$$\left| \frac{g}{g + j\omega} 0.5(1 + e^{-j\omega T_k N}) e^{-j\omega T_k} \right| \leq \left| \frac{g}{g + j\omega} \right| < \left| \frac{1}{W(e^{-j\omega T_k})} \right|, \quad \forall \omega.$$

The upper limit for  $g$  can be determined with this condition. The simple expression  $\left| \frac{g}{g + j\omega} \right| < \left| \frac{1}{W(e^{-j\omega T_k})} \right|$  provides a sufficient condition without considering the time delay element  $e^{-j\omega T_k N}$ .

### C. Comparison of PDOB with DOB

This subsection compares the PDOB with the DOB mentioned in [5]. The sensitivity function  $1 - Q(z^{-1})z^{-1}$  and the complementary sensitivity function  $Q(z^{-1})$  are used in the comparison because the sensitivity characteristic corresponds to the disturbance suppression characteristic. Moreover, the complementary sensitivity characteristic corresponds to the noise sensitivity and robust stability. The Bode diagrams of the PDOB and two types of DOB are shown in Fig. 5. DOB1 and DOB2 use the cutoff frequencies 100 rad/s and 25 rad/s, respectively. In the sensitivity functions shown in Fig. 5(a), the PDOB achieves the lowest gain for the periodic disturbance, which consists of a fundamental wave at 100 rad/s and harmonics at 200, 300, rad/s. Compared with DOB2, the PDOB includes not only the high-pass characteristic but also an infinite number of band-stop characteristics. Moreover, the complementary sensitivity characteristic of the PDOB shown in Fig. 5(b) has an infinite number of band-stop characteristics in addition to a low-pass characteristic in comparison with DOB1. Therefore, both periodic-disturbance suppression characteristic and gain of the complementary sensitivity function of the PDOB are better than those of DOB1. In comparison with DOB2, the PDOB improves the sensitivity function only at the frequencies of the periodic disturbance in the tradeoff.



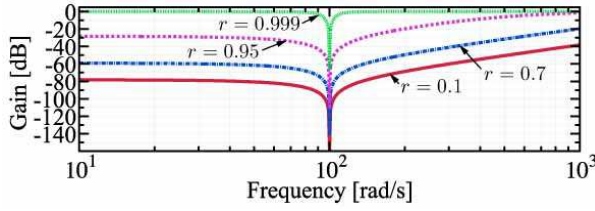


Fig. 7. Bode diagram of notch filter with variations in  $r$ . The other parameters are  $\xi = -2 \cos(100T_k)$  and  $T_k = 0.1$  ms.

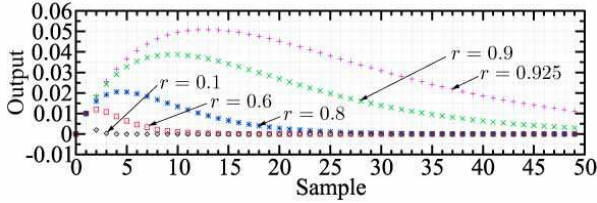


Fig. 8. Convergences of notch filter processing  $\sin(100T_k k)$  with variations in  $r$ . The other parameters are  $\xi = -2 \cos(100T_k)$  and  $T_k = 0.1$  ms.

A band-pass filter  $B(z^{-1}, \hat{\omega}_0)$  is used to provide a pure fundamental wave as the input to the ANF  $\tilde{d}$  from the output of the PDOB  $\varepsilon$ , which are shown in Fig. 6. This study uses the band-pass filter

$$B(j\omega, \hat{\omega}_0) = \left\{ \frac{j\omega g_b}{(\hat{\omega}_0^2 - \omega^2) + j\omega g_b} \right\}^2, \quad (11)$$

which has a design frequency  $g_b$  governing the bandwidth, as show in Fig. 9. The parameter  $g_b$  needs to be small when harmonics of a periodic disturbance are strong. The center frequency uses the fundamental frequency estimated by the ANF. In addition to the band-pass filter, the low-pass filter  $q_a(z^{-1})$  is used to suppress oscillations in the outputted fundamental frequency  $\hat{\omega}_0$  due to other elements in  $\tilde{d}$  that are not a fundamental wave. The cutoff frequency  $g_a$  of the low-pass filter  $q_a(z^{-1})$  is also a design frequency.

A numerical example is shown in Fig. 10. It uses the following controller, plant, and disturbance:

$$\begin{aligned} r(z^{-1}) &= - \left( 200 + 10000 \frac{T_k}{1 - z^{-1}} \right) y(z^{-1}), \\ y(z^{-1}) &= \frac{T_k}{1 - z^{-1}} \left[ \{r(z^{-1}) + \hat{d}_p(z^{-1})\} z^{-1} - d_p(z^{-1}) \right], \\ d_p(k) &= \begin{cases} \sin(100T_k k) & \text{if } T_k k < 10 \text{ s} \\ \sin(130T_k k) & \text{if } 10 \text{ s} \leq T_k k \end{cases}. \end{aligned}$$

The example validates the suppression characteristics of the PDOB and the adaptive PDOB.

### B. Convergence of Adaptive Algorithm

The convergence of the adaptive algorithm is described in this subsection. A stationary environment that assumes a forgetting factor  $\lambda$  of unity is considered. In addition,  $\tilde{d}(k)$  is assumed to be mainly composed of a fundamental wave. Then,  $\alpha(h)$  in the algorithm of the ANF mainly consists of a sinusoidal wave whose frequency is equal to that of the fundamental wave. It guarantees that  $\lim_{h \rightarrow \infty} 1/\{\sum_{n=1}^h \alpha^2(n)\}$

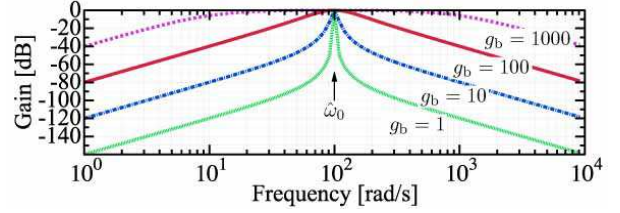


Fig. 9. Bode diagram of band-pass filter with variations in  $g_b$ . The other parameters are  $\hat{\omega}_0 = 100$  rad/s and  $T_k = 0.1$  ms.

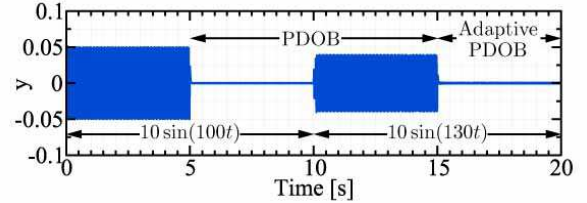


Fig. 10. Sinusoidal disturbance suppression using PDOB and adaptive PDOB. The parameters are  $\hat{\omega}_0(0) = 100$  rad/s,  $\gamma = 0.5$ ,  $g = 1000$  rad/s,  $r = 0.7$ ,  $\kappa = 10$ ,  $\lambda = 0.999$ ,  $\delta = 1000$ ,  $g_a = 1000$  rad/s,  $g_b = 1000$  rad/s, and  $T_k = 0.1$  ms.

converges to zero. Based on the convergence,  $P(h)$  in (14) also converges to zero with

$$\lim_{h \rightarrow \infty} P(h) = \lim_{h \rightarrow \infty} \frac{1}{\sum_{n=1}^h \alpha^2(n) + \delta} = 0.$$

Consequently, the gain  $g(h)$  in (17) becomes zero. Since  $P(h)$  and  $g(h)$  become zero in the steady-state, the steady-state  $\hat{\xi}(h)$  in (16) is

$$\hat{\xi}(h) = \hat{\xi}(h-1).$$

In conclusion, the convergences of  $P(h)$ ,  $g(h)$ , and  $\hat{\xi}(h)$  to zero and the steady-state are confirmed.

Next, the convergence of the adaptive variable  $\hat{\xi}(h)$  to the true value  $\xi(h)$  is described. From (13) and (14),  $\hat{\xi}(h)$  can be expressed by

$$\hat{\xi}(h) = \frac{\sum_{n=1}^h \alpha(n) \{\eta(n) - \beta(n)\}}{\sum_{n=1}^h \alpha^2(n) + \delta}. \quad (12)$$

Because the output of the unknown filter is

$$\eta(n) = \alpha(n)\xi + \beta(n) - w(n),$$

(12) can be rewritten as

$$\hat{\xi}(h) = \frac{\sum_{n=1}^h \alpha^2(n)}{\sum_{n=1}^h \alpha^2(n) + \delta} \xi - \frac{\sum_{n=1}^h \alpha(n)}{\sum_{n=1}^h \alpha^2(n) + \delta} w(n).$$

The parameter  $w(k)$  is noise effect due to  $v(k)$  with

$$\begin{aligned} w(k) &= \{-rw(k-1) + v(k-1)\}\xi \\ &\quad - r^2 w(k-2) + v(k) + v(k-2), \end{aligned}$$

and  $v(k)$  includes elements that are not a fundamental wave in  $\tilde{d}(k)$ , i.e., harmonics and aperiodic disturbances. The noise effect  $w(k)$  corresponds to the errors due to  $\eta = 0$ . In order to let  $\hat{\xi}(h)$  converge to the true value  $\xi(h)$ ,  $\frac{\sum_{n=1}^h \alpha^2(n)}{\sum_{n=1}^h \alpha^2(n) + \delta}$

and  $\frac{\sum_{n=1}^h \alpha(n)w(n)}{\sum_{n=1}^h \alpha^2(n) + \delta}$  need to be 1 and 0, respectively. The regularization parameter  $\delta$  adjusts them in the tradeoff: a small  $\delta$  sets the first term to 1 and a large  $\delta$  reduces the influence of  $w(n)$ . Another way to improve the convergence is to adjust the band-pass filter  $B(z^{-1}, \hat{\omega}_0)$ , which directly reduces the power of  $w(n)$ .

### C. Step Frequency Estimation Examples for Design of Six Additional Parameters

The design of the six additional design parameters  $r$ ,  $\kappa$ ,  $\lambda$ ,  $\delta$ ,  $g_a$ , and  $g_b$  is described in this subsection with step frequency estimations verifying several parameter examples. The estimation results are shown in Fig. 11 in which the output of the PDOB,  $\varepsilon$ , is set to

$$\varepsilon(k) = \begin{cases} \sin(100T_k k) & T_k k < 3 \text{ s} \\ \sin(110T_k k) & 3 \text{ s} \leq T_k k \end{cases}.$$

Fig. 11(a) shows that oscillations and overshoot occur when the notch parameter  $r$  is large. Hence, lower  $r$  values are preferred. After the determination of  $r$ , the multi-rate ratio  $\kappa$  can be determined from  $r$  and Fig. 8 as a sufficiently large value to wait for the convergence of the notch filter. Regarding the step frequency estimation shown in Fig. 11(b), a very small  $\kappa$  that induces an oscillating response is not suitable. The forgetting factor  $\lambda$  is usually selected as a positive value close to, but less than, unity. When set to a small value,  $\lambda$  deteriorates the transient response, as shown in Fig. 11(c). A design index of the regularization parameter  $\delta$  is described in Section III-B. A small  $\delta$  realizes high-speed response and a large  $\delta$  suppresses noise effect. Moreover, Fig. 11(d) demonstrates that the initial response is much affected by  $\delta$ . A large  $\delta$  causes a smooth response. In Figs. 11(e) and (f), the cutoff frequency  $g_a$  of the low-pass filter  $q_a(z^{-1})$  suppresses oscillations of the estimated fundamental frequency, and the design frequency  $g_b$  of the band-pass filter  $B(z^{-1}, \hat{\omega}_0)$  changes the transient response. However, the two parameters should be designed in accordance with the example of the fundamental-frequency estimation from a periodic disturbance including also harmonics. Fig. 12 shows step frequency estimations based on five combinations of  $g_a$  and  $g_b$ . The estimation uses an input including the fundamental frequency and ten harmonics:

$$\varepsilon(k) = \begin{cases} \sum_{n=1}^{10} \sin(n100T_k k) & T_k k < 3 \text{ s} \\ \sum_{n=1}^{10} \sin(n110T_k k) & 3 \text{ s} \leq T_k k \end{cases}.$$

According to Fig. 12, the cutoff frequency  $g_a$  suppresses the oscillations and the design frequency  $g_b$  modifies the steady-state accuracy. The problems typically occur due to strong harmonics and aperiodic disturbances. The frequencies  $g_a$  and  $g_b$  are determined with consideration of the characteristics and the convergence time.

## IV. SIMULATIONS

Two simulations to compare the PDOB with an RC and DOB and the PDOB with the adaptive PDOB were conducted.

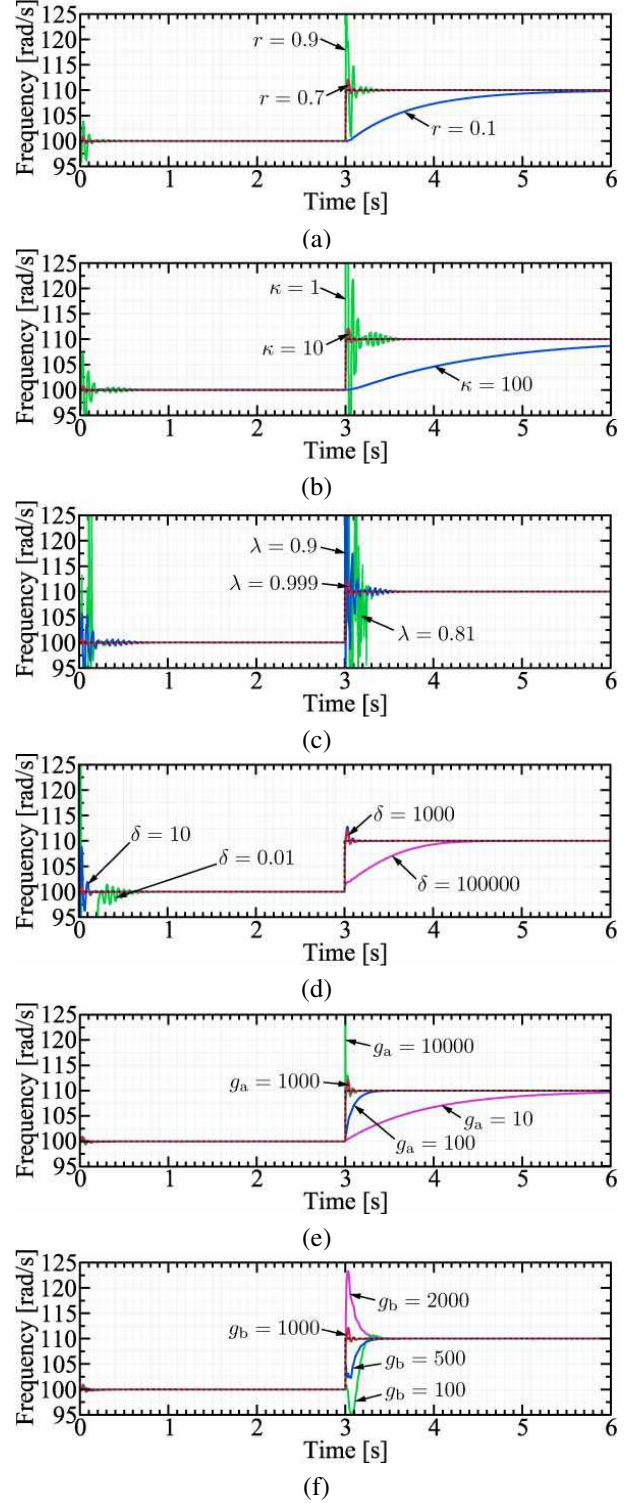


Fig. 11. Step frequency estimations for a sinusoidal wave. The standard parameters are  $\hat{\omega}_0(0) = 100$  rad/s,  $r = 0.7$ ,  $\kappa = 10$ ,  $\lambda = 0.999$ ,  $\delta = 1000$ ,  $g_a = 1000$  rad/s,  $g_b = 1000$  rad/s, and  $T_k = 0.1$  ms.

These controller, plant, and disturbance were assumed

$$\begin{aligned} I^{\text{ref}}(z^{-1}) &= -\frac{J}{K_t} (2500 + 100D(z^{-1})) x^{\text{res}}, \\ x^{\text{res}}(z^{-1}) &= \frac{1}{J} \left( \frac{T_k}{1 - z^{-1}} \right)^2 \\ &\quad \left[ \{K_t I^{\text{ref}}(z^{-1}) + \hat{d}_p(z^{-1})\} z^{-1} - d_p(z^{-1}) \right], \\ d_p &= \sum_{n=0}^{20} \sin(n\omega_0(k)T_k k), \end{aligned}$$

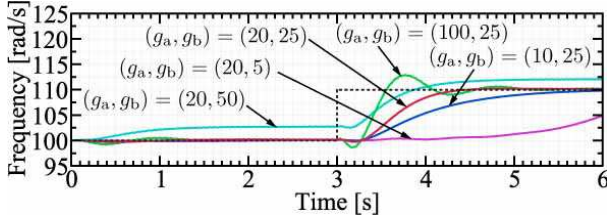


Fig. 12. Step frequency estimations for a periodic disturbance. The other parameters are  $\hat{\omega}_0(0) = 100$  rad/s,  $r = 0.7$ ,  $\kappa = 10$ ,  $\lambda = 0.999$ ,  $\delta = 1000$ , and  $T_k = 0.1$  ms.

TABLE II  
SIMULATION PARAMETERS.

Parameter	Symbol	Value
Sampling time	$T_k$	0.1 ms
Inertia	$J$	0.0028 kgm <sup>2</sup>
Torque constant	$K_t$	1.18 Nm/A
Initial fundamental freq.	$\omega_0(0)$	10 rad/s
Design parameter	$\gamma$	0.7
Cutoff freq. of $q(z^{-1})$	$g$	1000 rad/s
Notch parameter	$r$	0.7
Multi-rate ratio	$\kappa$	10
Forgetting factor	$\lambda$	0.999
Regularization parameter	$\delta$	1000
Cutoff freq. of $q_a(z^{-1})$	$g_a$	1 rad/s
Design freq. of $B(z^{-1})$	$g_b$	1 rad/s
Cutoff freq. for the DOB and RC	$g$	1000 rad/s

where  $D(z^{-1})$  is the pseudo differentiator. The parameters are shown in TABLE II. The modified RC with  $a = 1$  [10] and DOB [5] were used. The command was set to zero to validate only the disturbance suppression characteristics. The fundamental frequency  $\omega_0(k)$  was constantly set to 10 rad/s in Simulation 1. Simulation 2 used

$$\omega_0(k) = \begin{cases} 10 \text{ rad/s} & \text{if } 0 \leq T_k k < 40 \text{ s} \\ 11 \text{ rad/s} & \text{if } 40 \leq T_k k \end{cases}.$$

The results of Simulation 1 are shown in Fig. 13 and the transient responses of Fig. 13 are illustrated in Fig. 14. The steady-state characteristics are presented by using a discrete Fourier transform (DFT). The DFT results of Fig. 13 from 20 s - 100 s are shown in Fig. 15. In the transient response, the RC and PDOB need a storing process to be efficient due to their time delay elements. However, the PDOB achieves a better transient response than the RC. In the steady-state between 20 s - 100 s, the PDOB shows the better suppression performance at all frequencies of the periodic disturbance than that of the DOB.

The results of Simulation 2 are shown in Fig. 16. The fundamental-frequency estimation results of the adaptive PDOB are depicted in Fig. 17. The transient response of the adaptive estimation needs a long convergence time due to the harmonics between 40 s - 70 s. However, the adaptivity, which together with the estimation of the varying frequency achieves the best suppression performance, can be confirmed.

## V. EXPERIMENTS

Two experiments to compare the PDOB with an RC and DOB and the PDOB with the adaptive PDOB were conducted

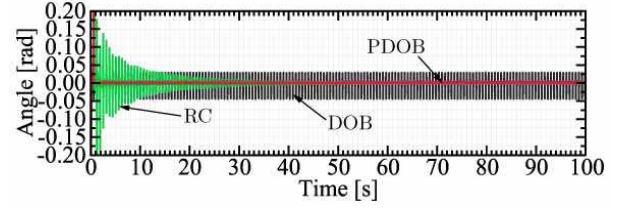


Fig. 13. Results of Simulation 1.

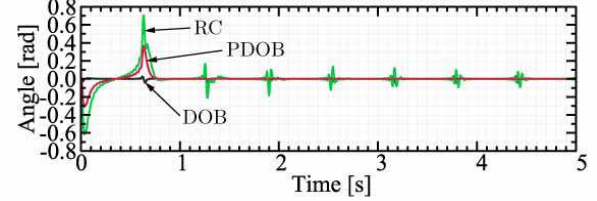


Fig. 14. Transient responses of Fig. 13.

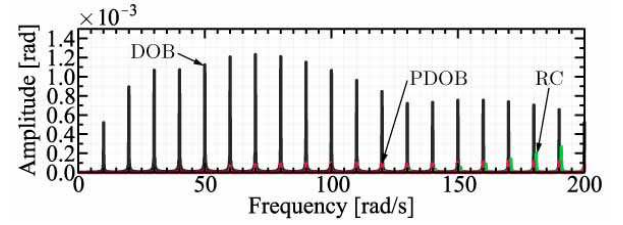


Fig. 15. DFT results of Fig. 13 for 20 s - 100 s.

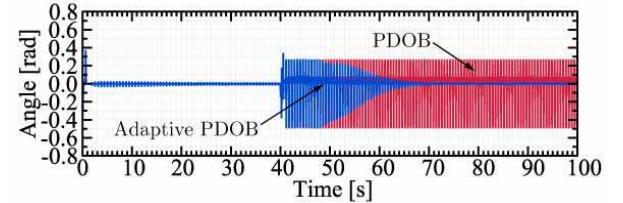


Fig. 16. Results of Simulation 2.

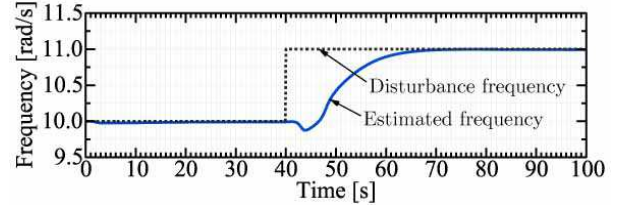


Fig. 17. Fundamental-frequency estimation result of adaptive PDOB.

with the multi-axis manipulator shown in Fig. 18. The parameters are summarized in TABLE III and the commands in the work space were given as

$$\begin{aligned} x^{\text{cmd}}(k) &= x_0 + 50 \cos\{\omega_0(k)T_k k\} - 50 \text{ mm} \\ y^{\text{cmd}}(k) &= y_0 + 50 \sin\{\omega_0(k)T_k k\} \text{ mm}, \end{aligned}$$

TABLE III  
EXPERIMENTAL PARAMETERS.

Parameter	Symbol	Value (1st, 2nd, 3rd) Joint
Sampling time	$T_k$	0.1 ms
Proportional gain	$K_P$	(400, 400, 400)
Differential gain	$K_D$	(40, 40, 40)
Nominal inertia	$J_n$	(7.0, 3.0, 0.3) kgm <sup>2</sup>
Nominal torque constant	$K_{tn}$	(0.59, 0.59, 0.238) Nm/A
Gear ratio	$G_r$	(192, 120, 80)
Length	$L$	(0.26, 0.27, 0.09) m
Identified fundamental freq.	$\omega_0(0)$	(3, 3, 3) rad/s
Design parameter	$\gamma$	(0.5, 0.5, 0.5)
Cutoff freq. of $q(z^{-1})$	$g$	(200, 200, 200) rad/s
Notch parameter	$r$	(0.1, 0.1, 0.1)
Multi-rate ratio	$\kappa$	(10, 10, 10)
Forgetting factor	$\lambda$	(0.999, 0.999, 0.999)
Regularization parameter	$\delta$	(10 <sup>7</sup> , 10 <sup>7</sup> , 10 <sup>7</sup> )
Cutoff freq. of $q_a(z^{-1})$	$g_a$	(1, 1, 1) rad/s
Design freq. of $B(z^{-1})$	$g_b$	(2, 2, 2) rad/s
Cutoff freq. for the DOB	$g$	(200, 200, 200) rad/s
Cutoff freq. for the RC	$g$	(30, 30, 30) rad/s

TABLE IV  
RMSES OF EXPERIMENTAL RESULTS.

Experiment 1	DOB	RC + DOB	PDOB + DOB
$x$ -axis	0.256 mm	0.157 mm	0.066 mm
$y$ -axis	0.277 mm	0.150 mm	0.073 mm
Experiment 2	PDOB + DOB	Adaptive PDOB + DOB	
$x$ -axis	0.191 mm	0.117 mm	
$y$ -axis	0.236 mm	0.127 mm	



Fig. 18. Experimental multi-axis manipulator.

where  $x_0$  and  $y_0$  are the initial positions. In Experiment 1, the command frequency  $\omega_0(k)$  was constantly set to 3 rad/s. In Experiment 2, it was set to

$$\omega_0(k) = \begin{cases} 3 \text{ rad/s} & \text{if } 0 \leq T_k k < 40 \\ 4 \text{ rad/s} & \text{if } 45 \leq T_k k \end{cases}.$$

In the shifting phase of 40 s - 45 s, a smooth command that shifts  $x_1^{\text{cmd}}$  to  $x_2^{\text{cmd}}$  was given as

$$x^{\text{cmd}} = x_1^{\text{cmd}} + (x_2^{\text{cmd}} - x_1^{\text{cmd}})(T_k k - 40)/(45 - 40).$$

In the experimental control systems, the modified RC with  $a = 1$  [10] and DOB [5] were applied. All control methods were implemented with a proportional-derivative controller and a feedforward controller that sets the input-output transfer function to 1. Hence, the experimental errors depend only on disturbance suppression characteristics. More specifically, the RC, PDOB, and adaptive PDOB were implemented with the DOB because they do not compensate aperiodic disturbances.

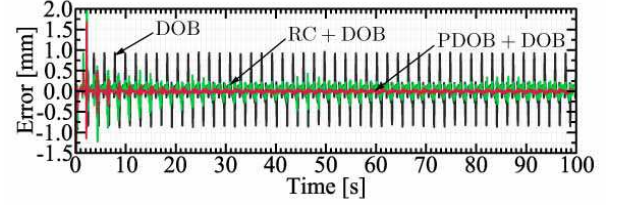


Fig. 19. Error values regarding  $y$ -axis of Experiment 1.

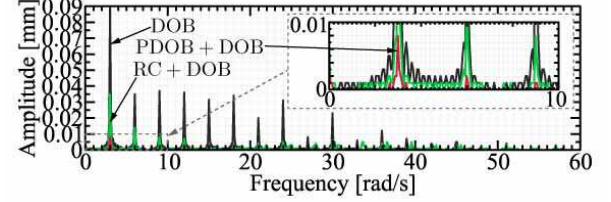


Fig. 20. DFT results of Fig. 19 from 20 s - 100 s.

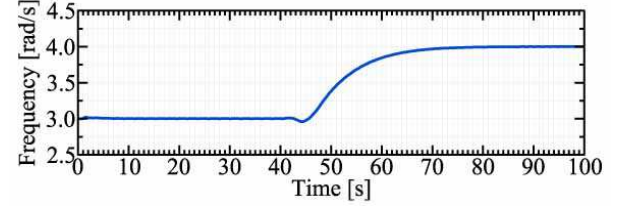


Fig. 21. Fundamental-frequency estimation result of adaptive PDOB implemented at first joint.

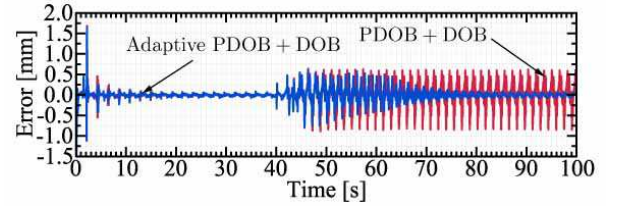


Fig. 22. Error values regarding  $y$ -axis of Experiment 2.

The root-mean-square errors (RMSEs) of the experimental results are shown in TABLE IV. The error values regarding the  $y$ -axis of Experiment 1 are shown in Fig. 19. In the transient response, the RC and PDOB require storing time to be efficient because of their time delay elements. In the steady-state, the PDOB and DOB combination performs the best periodic-disturbance suppression. The DFT results of Fig. 19 are shown in Fig. 20. They demonstrate that the PDOB with DOB achieve suppression of all fundamental wave and harmonics in the frequency domain. Further, the PDOB does not deteriorate the compensation by the DOB, whereas the RC amplifies the other disturbances for frequencies between those of the periodic disturbance in the frequency domain larger than 20 rad/s. In Experiment 2, the compensation of the frequency-varying periodic disturbance was validated. The adaptivity estimated the fundamental frequency of the

periodic disturbance, as shown in Fig. 21, and maintains the best suppression performance of the PDOB. The error values regarding the  $y$ -axis are shown in Fig. 22. In the steady-state, the adaptive PDOB achieves the best performance of the PDOB. However, the adaptive estimation and the performance improvement need a long convergence time.

## VI. CONCLUSION

The PDOB and adaptive PDOB were proposed in this paper. The PDOB was constructed to compensate a periodic disturbance with three parameters: a fundamental frequency of a periodic disturbance  $\omega_0$ , design parameter  $\gamma$ , and cutoff frequency  $g$ . Because the fundamental frequency  $\omega_0$  needs preidentification, the adaptive PDOB including an ANF was also proposed with six additional design parameters: a notch parameter  $r$ , multi-rate ratio  $\kappa$ , forgetting factor  $\lambda$ , regularization parameter  $\delta$ , cutoff frequency  $g_a$ , and design frequency  $g_b$ . The adaptivity causes the PDOB to achieve the best performance and realizes a compensation of frequency-varying periodic disturbances by estimating the fundamental frequency of a periodic disturbance.

## APPENDIX A

### DERIVATION OF ADAPTIVE ALGORITHM

This appendix presents the derivation of the ANF algorithm. The ANF is expressed with  $\hat{\eta}(k) = \alpha(k)\hat{\xi}(k) + \beta(k)$ , as shown in TABLE I. The algorithm for the adaptive variable  $\hat{\xi}(h)$  is obtained in accordance with the minimization of the cost function in (10) with respect to  $\hat{\xi}(h)$ . The condition  $\frac{\partial J(h)}{\partial \hat{\xi}(h)} = 0$ , which satisfies the minimization of the cost function, provides

$$2 \sum_{n=1}^h \lambda^{h-n} \alpha(n) \{ \eta(n) - \alpha(n)\hat{\xi}(h) - \beta(n) \} - 2\delta \lambda^h \hat{\xi}(h) = 0.$$

The  $\hat{\xi}(h)$  satisfying  $\frac{\partial J(h)}{\partial \hat{\xi}(h)} = 0$  is obtained with

$$\hat{\xi}(h) = P(h) \sum_{n=1}^h \lambda^{h-n} \alpha(n) \{ \eta(n) - \beta(n) \}, \quad (13)$$

where  $P(h)$  is

$$P(h) = \frac{1}{\sum_{n=1}^h \lambda^{h-n} \alpha^2(n) + \delta \lambda^h}. \quad (14)$$

From (14), the recursive  $P^{-1}(h)$  is derived as

$$P^{-1}(h) = \lambda P^{-1}(h-1) + \alpha^2(h). \quad (15)$$

Further, (13) is transformed into

$$\hat{\xi}(h) = \hat{\xi}(h-1) + P(h)\alpha(h)e(h).$$

The calculation of  $\hat{\xi}(h)$  for the algorithm is obtained as

$$\hat{\xi}(h) = \hat{\xi}(h-1) + g(h)e(h), \quad (16)$$

where the gain  $g(h)$  is

$$g(h) = P(h)\alpha(h). \quad (17)$$

The adaptive error is calculated with  $e(h) = \eta(h) - \hat{\eta}(h)$ , and the gain is rewritten by substituting (15) with (17) for a recursive equation

$$g(h) = \frac{P(h-1)\alpha(h)}{\lambda + P(h-1)\alpha^2(h)}. \quad (18)$$

$P(h)$  is further rewritten with (15) and (18) as

$$P(h) = \frac{1}{\lambda} \{ P(h-1) - g(h)\alpha(h)P(h-1) \}.$$

## ACKNOWLEDGMENT

This work was partially supported by JSPS KAKENHI.

## REFERENCES

- [1] W. H. Chen, J. Yang, L. Guo, and S. Li, "Disturbance-observer-based control and related methods—an overview," *IEEE Trans. Ind. Electron.*, vol. 63, no. 2, pp. 1083–1095, Feb. 2016.
- [2] K. Ohnishi, M. Shibata, and T. Murakami, "Motion control for advanced mechatronics," *IEEE/ASME Trans. Mechatronics*, vol. 1, no. 1, pp. 56–67, Mar. 1996.
- [3] M. Ruderman, A. Ruderman, and T. Bertram, "Observer-based compensation of additive periodic torque disturbances in permanent magnet motors," *IEEE Trans. Ind. Informat.*, vol. 9, no. 2, pp. 1130–1138, May 2013.
- [4] K. Natori, R. Oboe, and K. Ohnishi, "Stability analysis and practical design procedure of time delayed control systems with communication disturbance observer," *IEEE Trans. Ind. Informat.*, vol. 4, no. 3, pp. 185–197, Aug. 2008.
- [5] E. Sariyildiz and K. Ohnishi, "Stability and robustness of disturbance-observer-based motion control systems," *IEEE Trans. Ind. Electron.*, vol. 62, no. 1, pp. 414–422, Jan. 2015.
- [6] J. N. Yun and J. B. Su, "Design of a disturbance observer for a two-link manipulator with flexible joints," *IEEE Trans. Control Syst. Technol.*, vol. 22, no. 2, pp. 809–815, Mar. 2014.
- [7] J. Karttunen, S. Kallio, P. Peltoniemi, and P. Silventoinen, "Current harmonic compensation in dual three-phase PMSMs using a disturbance observer," *IEEE Trans. Ind. Electron.*, vol. 63, no. 1, pp. 583–594, Jan. 2016.
- [8] W. Kim, D. Shin, D. Won, and C. C. Chung, "Disturbance-observer-based position tracking controller in the presence of biased sinusoidal disturbance for electrohydraulic actuators," *IEEE Trans. Control Syst. Technol.*, vol. 21, no. 6, pp. 2290–2298, Nov. 2013.
- [9] K. Cho, J. Kim, S. B. Choi, and S. Oh, "A high-precision motion control based on a periodic adaptive disturbance observer in a PMLSM," *IEEE/ASME Trans. Mechatronics*, vol. 20, no. 5, pp. 2158–2171, Oct. 2015.
- [10] S. Hara, Y. Yamamoto, T. Omata, and M. Nakano, "Repetitive control system: a new type servo system for periodic exogenous signals," *IEEE Trans. Autom. Control*, vol. 33, no. 7, pp. 659–668, Jul. 1988.
- [11] Y. Yang, K. Zhou, and M. Cheng, "Phase compensation resonant controller for PWM converters," *IEEE Trans. Ind. Informat.*, vol. 9, no. 2, pp. 957–964, May 2013.
- [12] H. Fujimoto, "RRO compensation of hard disk drives with multirate repetitive perfect tracking control," *IEEE Trans. Ind. Electron.*, vol. 56, no. 10, pp. 3825–3831, Oct. 2009.
- [13] Y.-S. Lu, S.-M. Lin, M. Hauschild, and G. Hirzinger, "A torque-ripple compensation scheme for harmonic drive systems," *Electrical Eng.*, vol. 95, no. 4, pp. 357–365, Dec. 2013.
- [14] X. Chen and M. Tomizuka, "New repetitive control with improved steady-state performance and accelerated transient," *IEEE Trans. Control Syst. Technol.*, vol. 22, no. 2, pp. 664–675, Mar. 2014.
- [15] J. Han, "From PID to active disturbance rejection control," *IEEE Trans. Ind. Electron.*, vol. 56, no. 3, pp. 900–906, Mar. 2009.
- [16] Q.-C. Zhong and D. Rees, "Control of uncertain LTI systems based on an uncertainty and disturbance estimator," *ASME J. Dyn. Sys., Meas., Control*, vol. 126, no. 4, pp. 905–910, Dec. 2004.
- [17] S. Jafari and P. A. Ioannou, "Rejection of unknown periodic disturbances for continuous-time MIMO systems with dynamic uncertainties," *Int. J. Adapt. Control Signal Process.*, vol. 30, no. 12, pp. 1674–1688, Dec. 2016.

- [18] I. D. Landau, A. C. Silva, T.-B. Airimitoie, G. Buche, and M. Noë, "Benchmark on adaptive regulation-rejection of unknown/time-varying multiple narrow band disturbances," *Eur. J. Control*, vol. 19, no. 4, pp. 237–252, Jul. 2013.
- [19] W. He and S. S. Ge, "Cooperative control of a nonuniform gantry crane with constrained tension," *Automatica*, vol. 66, pp. 146 – 154, Apr. 2016.
- [20] W. He, Y. Chen, and Z. Yin, "Adaptive neural network control of an uncertain robot with full-state constraints," *IEEE Trans. Cybern.*, vol. 46, no. 3, pp. 620–629, Mar. 2016.
- [21] I. D. Landau, M. Alma, A. Constantinescu, J. J. Martinez, and M. Noë, "Adaptive regulation-rejection of unknown multiple narrow band disturbances (a review on algorithms and applications)," *Control Eng. Practice*, vol. 19, no. 10, pp. 1168–1181, Oct. 2011.
- [22] M. Steinbuch, "Repetitive control for systems with uncertain period-time," *Automatica*, vol. 38, no. 12, pp. 2103–2109, Dec. 2002.
- [23] M. Mojiri and A. R. Bakhshai, "An adaptive notch filter for frequency estimation of a periodic signal," *IEEE Trans. Autom. Control*, vol. 49, no. 2, pp. 314–318, Feb. 2004.
- [24] R. Marino and P. Tomei, "Adaptive notch filters are local adaptive observers," *Int. J. Adapt. Control Signal Process.*, vol. 30, no. 1, pp. 128–146, Jan. 2016.
- [25] S. Haykin, *Adaptive Filter Theory*, 5th ed. Prentice-Hall, 2014.



**Hisayoshi Muramatsu (S'16)** received the B.E. degree in system design engineering and the M.E. degrees in integrated design engineering from Keio University, Yokohama, Japan, in 2016 and 2017, respectively. He is currently working toward the Ph.D. degree in integrated design engineering from Keio University, Yokohama, Japan. His research interests include motion control and mechatronics.



**Seiichiro Katsura (S'03-M'04)** received the B.E. degree in system design engineering and the M.E. and Ph.D. degrees in integrated design engineering from Keio University, Yokohama, Japan, in 2001, 2002 and 2004, respectively.

From 2003 to 2005, he was a Research Fellow of the Japan Society for the Promotion of Science (JSPS). From 2005 to 2008, he worked at Nagaoka University of Technology, Nagaoka, Niigata, Japan. Since 2008, he has been at Keio University, Yokohama, Japan. In 2017, he was a Visiting Researcher

with The Laboratory for Machine Tools and Production Engineering (WZL) of RWTH Aachen University, Aachen, Germany. His research interests include applied abstraction, human support, wave system, systems energy conversion, and electromechanical integration systems.

Prof. Katsura serves as an Associate Editor of the IEEE Transactions on Industrial Electronics. He was the recipient of The Institute of Electrical Engineers of Japan (IEEJ) Distinguished Paper Awards in 2003 and 2017, IEEE Industrial Electronics Society Best Conference Paper Award in 2012, and JSPS Prize in 2016.